The effect of a dynamo-generated field on the Parker wind

NORDITA ASTROPHYSICS SEMINARS

NORDITA

The Nordic Institute for Theoretical Physics

Patrik Jakab

Erasmus+

2020.06.10

Stockholm, Sweden

Content

- Introduction
- The model
- Results
- Conclusion

Astronomy & Astrophysics manuscript no. paper
June 5, 2020

The effect of a dynamo-generated field on the Parker wind

P. Jakab[1,2] and A. Brandenburg[1,3,4,5]

[1] Nordita, KTH Royal Institute of Technology and Stockholm University, Roslagstullsbacken 23, 10691 Stockholm, Sweden
[2] Department of Nuclear Physics and Subnuclear Physics, Pavol Jozef Safarik University in Kosice, Jesenna 5, 041 54 Kosice, Slovakia
[3] Department of Astronomy, AlbaNova University Center, Stockholm University, 10691 Stockholm, Sweden
[4] JILA and Laboratory for Atmospheric and Space Physics, University of Colorado, Boulder, CO 80303, USA
[5] McWilliams Center for Cosmology & Department of Physics, Carnegie Mellon University, Pittsburgh, PA 15213, USA

June 5, 2020, Revision: 1.69

ABSTRACT

Context. Stellar winds are an integral part of the underlying dynamo, the motor of stellar activity. The wind controls the star's angular momentum loss, which depends on the magnetic field geometry which, in turn, varies significantly in time and latitude.
Aims. Here we study basic properties of a self-consistent model that includes simple representations of both the global stellar dynamo in a spherical shell and the exterior in which the wind accelerates and becomes supersonic.
Methods. We numerically solve an axisymmetric mean-field model for the induction, momentum, and continuity equations using an isothermal equation of state. The model allows for the simultaneous generation of a mean magnetic field and the development of a Parker wind. The resulting flow is transonic at the critical point, which we arrange to be between the inner and outer radii of the model. The boundary conditions are assumed to be such that the magnetic field is antisymmetric about the equator, i.e., dipolar.
Results. At the solar rotation rate, the dynamo is oscillatory and of α^2 type. In most of the domain, the magnetic field corresponds to that of a split monopole. The magnetic energy flux is largest between the stellar surface and the critical point. At rapid rotation of up to 50 times the solar value, most of the magnetic field is lost along the axis within the inner tangential cylinder of the model.
Conclusions. The model reveals unexpected features that are not generally anticipated from models that are designed to reproduce the solar wind: highly variable angular momentum flux fluxes even from just an α^2 dynamo in the star. For rapid rotation, magnetic fields are ejected mostly along the axis, where the wind speed is reduced.

Key words. Sun: sunspots – Sun: dynamo – turbulence – magnetohydrodynamics (MHD) – hydrodynamics

1. Introduction

The emergence of a wind around stars is a remarkable and somewhat counter-intuitive phenomenon. The existence of the solar wind was already suggested by the fact that the tails of comets always point away from the Sun (Biermann 1951). Nevertheless, the wind was thought to be a relatively slow phenomenon associated with an evaporation of the corona (Chamberlain 1960). The physical nature and mathematical theory of the solar wind was first understood by Parker (1958). His theory showed that the wind starts off as a subsonic flow some distance above the corona. It gradually gains in speed as the gravitational force diminishes and the effective outward pull resulting from the quadratic increase of the cross-sectional area in Bernoulli's law. This is a purely hydrodynamic phenomenon, unlike what was suggested by the popular notion of the solar corpuscular radiation at the time.

Stellar winds play a crucial role in a star's life. Without the wind, the Sun would still be spinning rapidly and magnetically superactive. A proper understanding of the rotational evolution of a star through magnetic breaking via a wind is important not only for stellar evolution, but it also plays a role in understanding the diversity of magnetic activity as a function of rotation rate and age (van Saders et al. 2016). As the star reaches the age of the Sun, the magnetic field either changes its geometry such that stellar breaking is reduced (See et al. 2019; Metcalfe & van Saders 2017) or it can continue to break and the star's differential rotation becomes antisolar-like (Gastine et al. 2014; Käpylä et al. 2014), i.e., the equator spins slower than the poles. Stellar winds can also be important for the dynamo itself in that they can transport magnetic helicity away from the dynamo region, and thereby alleviate what is known as catastrophic quenching; see Mitra et al. (2011) for mean-field models and Del Sordo et al. (2013) for computations of the magnetic helicity flux in simulations in a turbulent wind. Magnetic winds also affect the density and dynamics of cosmic rays in the heliosphere. Computing selfconsistently the dynamo-generated magnetic field evolution in the heliosphere is therefore crucial and for modeling the magnetic shielding of Galactic cosmic rays on the Earth.

The theory of a magnetized stellar wind by Weber & Davis (1967) employes a prescribed and time-independent stellar magnetic field, so any feedback on the underlying dynamics was ignored. This is also true of the recent numerical models of Réville et al. (2015), who compared different magnetic multipoles as initial conditions of their models. This has changed only in recent years. Given that the wind normally dominates over the magnetic field, one can separate the dynamics of the wind from that of the solar dynamo. In recent work of Perri et al. (2018), this was modeled using two separate codes that are magnetically coupled through a matching condition at the solar surface.

The purpose of the present paper is to explore some basic properties of stellar winds in the presence of dynamo-generated magnetic fields. It is appropriate to adopt a mean-field model, where we solve the equations for the azimuthally averaged mag-

Introduction

Solar wind

https://science.howstuffworks.com/dictionary/astronomy-terms/solar-wind-info.htm

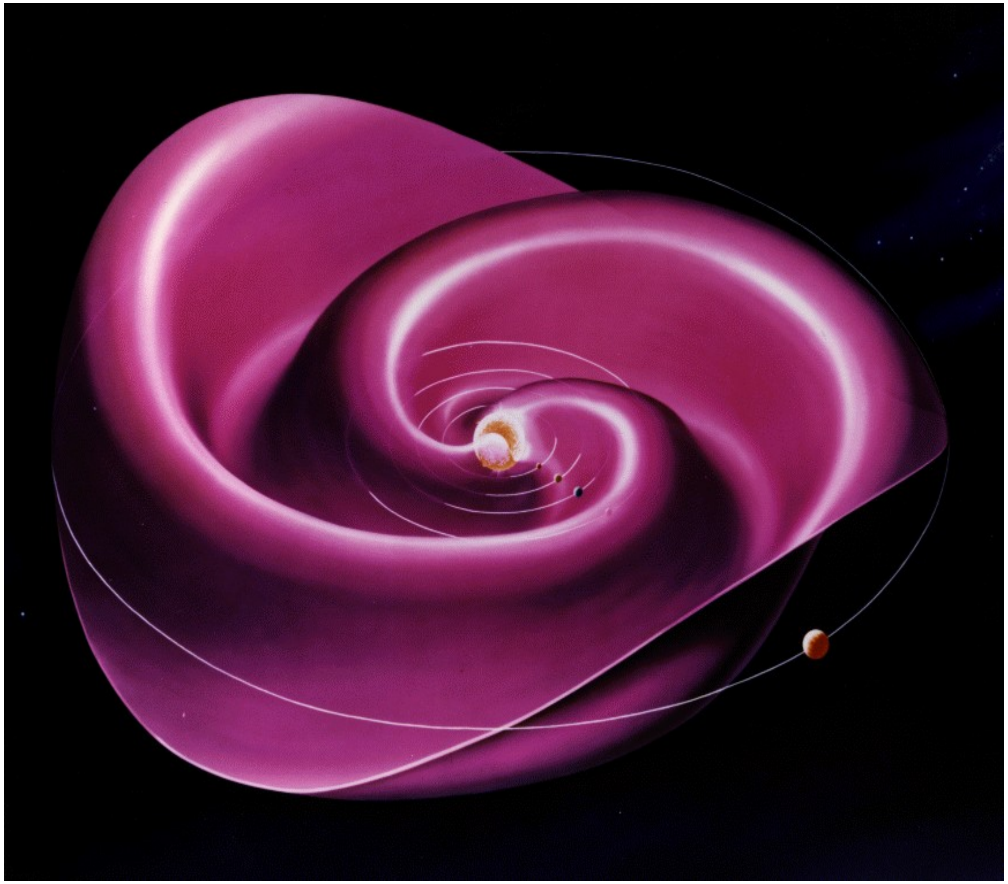

https://en.wikipedia.org/wiki/Heliospheric_current_sheet#/media/File:Heliospheric-current-sheet.gif

Introduction

$$C(r,u) = \tfrac{1}{2}u^2 - \ln r^2 - \ln u - \frac{1}{r}.$$

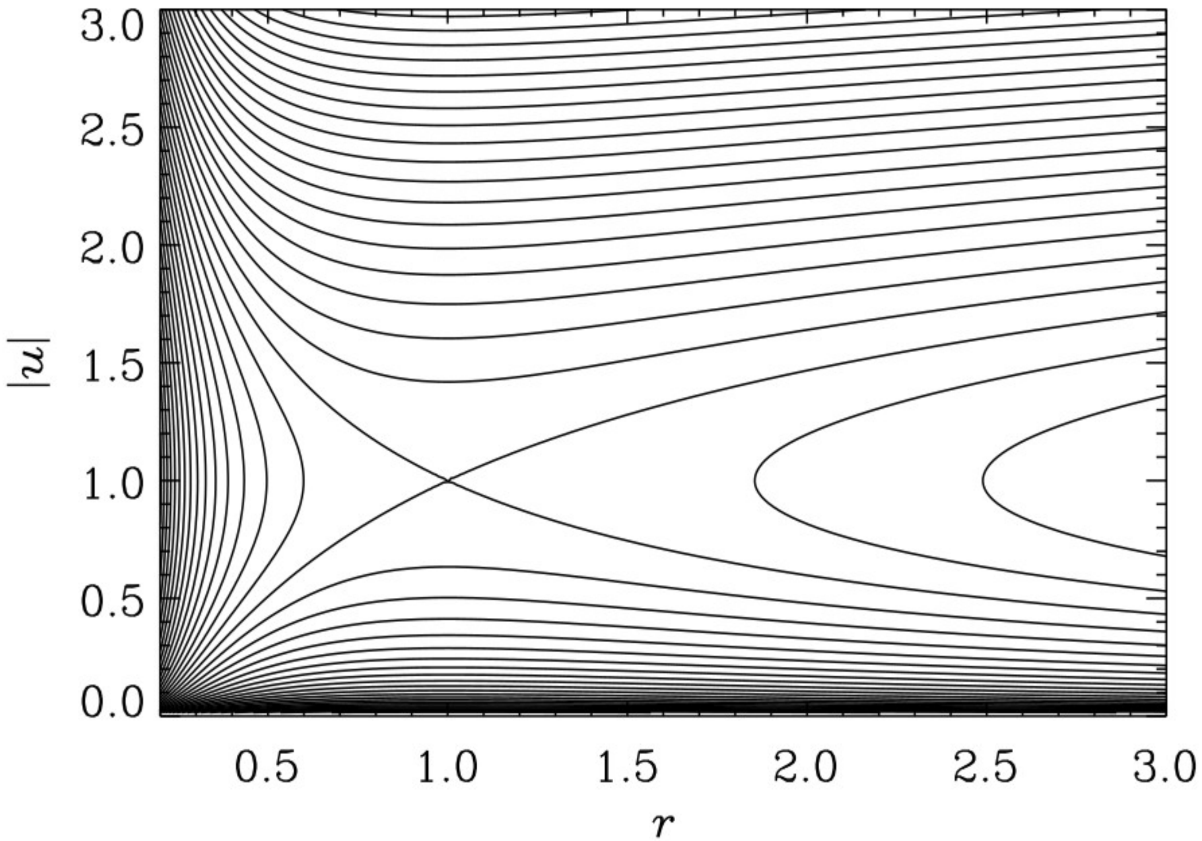

Contours of C(r, u)

Parker E. N., 1965

The model

Basic equations:

- evolution equation for the mean vector potential

$$\frac{\partial \overline{\boldsymbol{A}}}{\partial t} = \overline{\boldsymbol{U}} \times \overline{\boldsymbol{B}} + \alpha \overline{\boldsymbol{B}} - \eta_{\mathrm{T}} \overline{\boldsymbol{J}}, \tag{1}$$

- evolution equation for mean velocity

$$\frac{\mathrm{D}\overline{\boldsymbol{U}}}{\mathrm{D}t} = -c_{\mathrm{s}}^2 \boldsymbol{\nabla} \ln \overline{\rho} - \frac{GM}{r^2}\hat{\boldsymbol{r}} + \frac{1}{\overline{\rho}} \overline{\boldsymbol{J}} \times \overline{\boldsymbol{B}} - \nu_{\mathrm{T}} \overline{\boldsymbol{Q}}, \tag{2}$$

- evolution equation for logarithmic mean density

$$\frac{\mathrm{D} \ln \overline{\rho}}{\mathrm{D}t} = -\boldsymbol{\nabla} \cdot \overline{\boldsymbol{U}}, \tag{3}$$

$$\mathrm{D}/\mathrm{D}t = \partial/\partial t + \overline{\boldsymbol{U}} \cdot \boldsymbol{\nabla}$$

- mean current density

$$\overline{\boldsymbol{J}} = \boldsymbol{\nabla} \times \overline{\boldsymbol{B}}/\mu_0$$

$$-\overline{\boldsymbol{Q}} = \nabla^2 \overline{\boldsymbol{U}} + \tfrac{1}{3} \boldsymbol{\nabla}\boldsymbol{\nabla} \cdot \overline{\boldsymbol{U}} + 2\overline{\mathsf{S}} \cdot \boldsymbol{\nabla} \ln(\nu_{\mathrm{T}} \overline{\rho}) \tag{4}$$

- strain tensor of the mean flow

$$\overline{\mathsf{S}}_{ij} = \tfrac{1}{2}(\overline{U}_{i,j} + \overline{U}_{j,i}) - \tfrac{1}{3}\delta_{ij} \boldsymbol{\nabla} \cdot \overline{\boldsymbol{U}}$$

- quenching function for alpha effect

$$\alpha(r, \theta, \overline{\boldsymbol{B}}) = \frac{\alpha_0 f_\alpha(r) \cos\theta \sin^n \theta}{1 + Q_\alpha \overline{\boldsymbol{B}}^2 / B_{\mathrm{eq}}^2}, \tag{5}$$

- radial profile function

$$f_\alpha(r) = \Theta\Big((r - R)/w_\alpha\Big) \tag{6}$$

The model

3 distinct layers:

$$r_{\rm in} < R < r_* < r_{\rm out}, \tag{7}$$

where $r_{\rm in} < r < R$ is the dynamo region (modeling the stellar envelope), $R < r < r_*$ is the wind acceleration region (modeling the locations of the solar corona and the Alfvén point), and $r_* < r < r_{\rm out}$ is the supersonic wind region with $r_* = GM/2c_{\rm s}^2$ being the critical point.

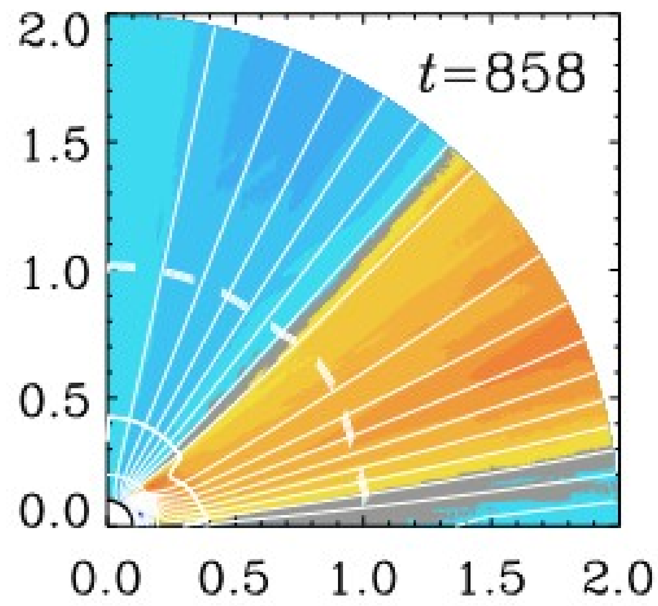

Boundary conditions:

$$\frac{\partial \overline{A}_r}{\partial r} = \overline{A}_\theta = \overline{A}_\phi = 0 \quad \text{on } r = r_{\rm in}, \tag{8}$$

$$\overline{A}_r = \frac{\partial \overline{A}_\theta}{\partial r} + \frac{\overline{A}_\theta}{r} = \frac{\partial \overline{A}_\phi}{\partial r} + \frac{\overline{A}_\phi}{r} = 0 \quad \text{on } r = r_{\rm out}. \tag{9}$$

$$\frac{\partial \overline{A}_r}{\partial \theta} = \overline{A}_\theta = \overline{A}_\phi = 0 \quad \text{on } \theta = 0^\circ , \tag{10}$$

$$\frac{\partial \overline{A}_r}{\partial \theta} = \overline{A}_\theta = \frac{\partial \overline{A}_\phi}{\partial \theta} = 0 \quad \text{on } \theta = 90^\circ . \tag{11}$$

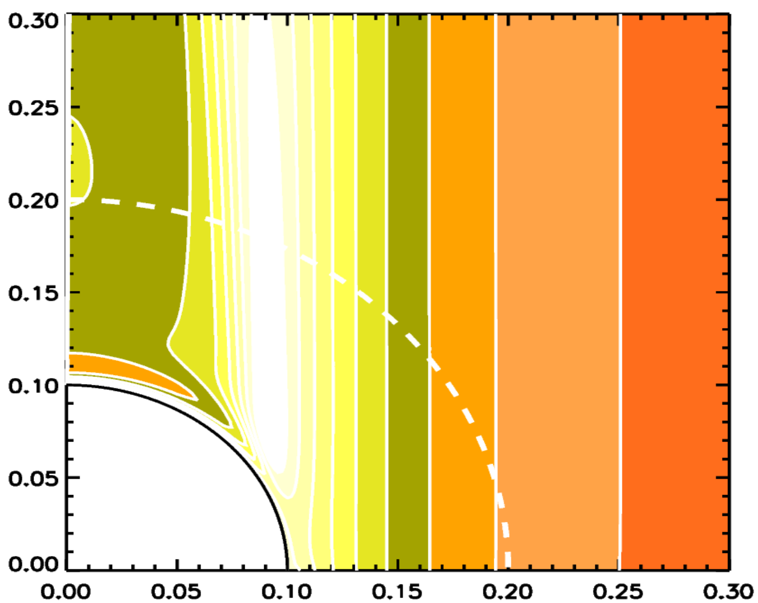

Wind solution as initial condition

Bernoulli equation:

$$\frac{1}{2}u^2 + c_s^2 \ln \overline{\rho} - GM/r = \text{const}, \qquad (12)$$

Mass loss rate:

$$\dot{M} = 4\pi r^2 \overline{\rho} u$$

$$\frac{1}{2}u^2 - c_s^2 \ln u - c_s^2 \ln r^2 - GM/r = \Phi_0, \qquad (13)$$

$r \leq r_*,\ u = c_s r/r_*$:

$$c_s^2 \ln u_{i+1}(r) = \frac{1}{2}u_i^2 - c_s^2 \ln r^2 - GM/r - \Phi_0, \qquad (14)$$

$r > r_*,\ u_0 = 2c_s$:

$$\frac{1}{2}u_{i+1}^2(r) = c_s^2 \ln u_i + c_s^2 \ln r^2 + GM/r + \Phi_0. \qquad (15)$$

The model

Wind solution as initial condition

https://www.nordita.org/~brandenb/teach/PencilCode/MixedTopics.html

Parker Wind

→ Working material: ParkerWind/, ParkerWind.tar.gz [untar this file by typing tar zxf ParkerWind.tar.gz]

The isothermal Parker wind is a solution of the equations

```
u du/dr = -cs^2 dlnrho/dr - GM/r^2 and
d(r^2 rho ur)/dr = 0
```

There is a critical point at r=GM/2cs^2. The numerical solution approaches the wind after some equilibration process. The inital condition was just ur=1.

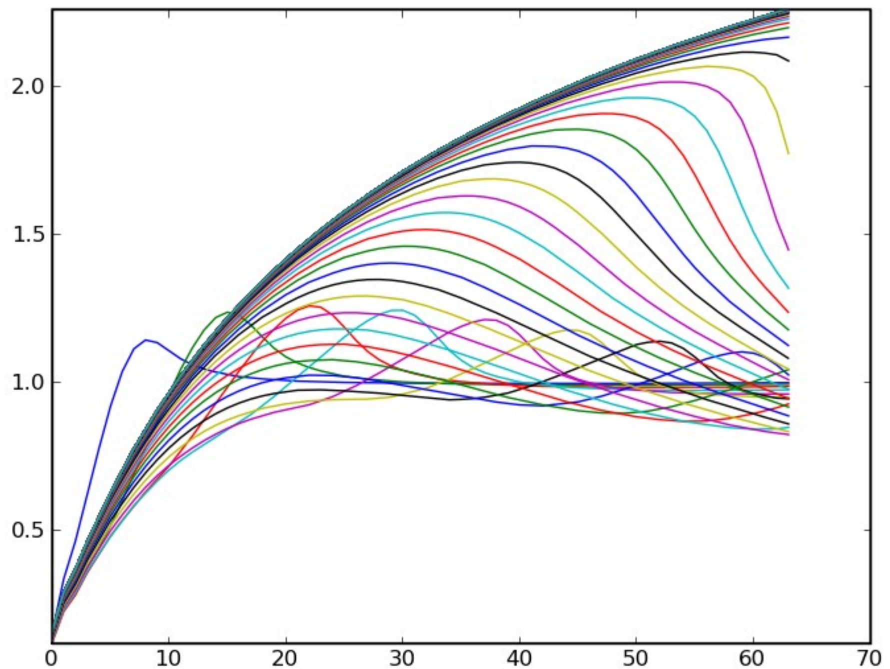

Jörn Warnecke and
Dhrubaditya Mitra, 2012

The model

Effective solar wind potential

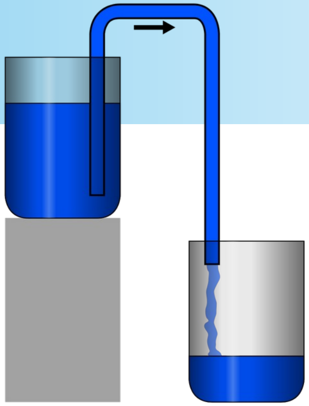

https://en.wikipedia.org/wiki/Siphon#/media/File:Lappo.svg

1D Bernoulli equation:

$$\left(u^2 - c_s^2\right) \frac{\mathrm{d}}{\mathrm{d}r} \ln u^2 = -\frac{\mathrm{d}\Phi_{\text{eff}}}{\mathrm{d}r},$$

Effective gravitational potential:

$$\Phi_{\text{eff}} = -c_s^2 \ln r^2 - GM/r,$$

-the effective potential experienced
by the siphon flow in the isothermal
Parker wind

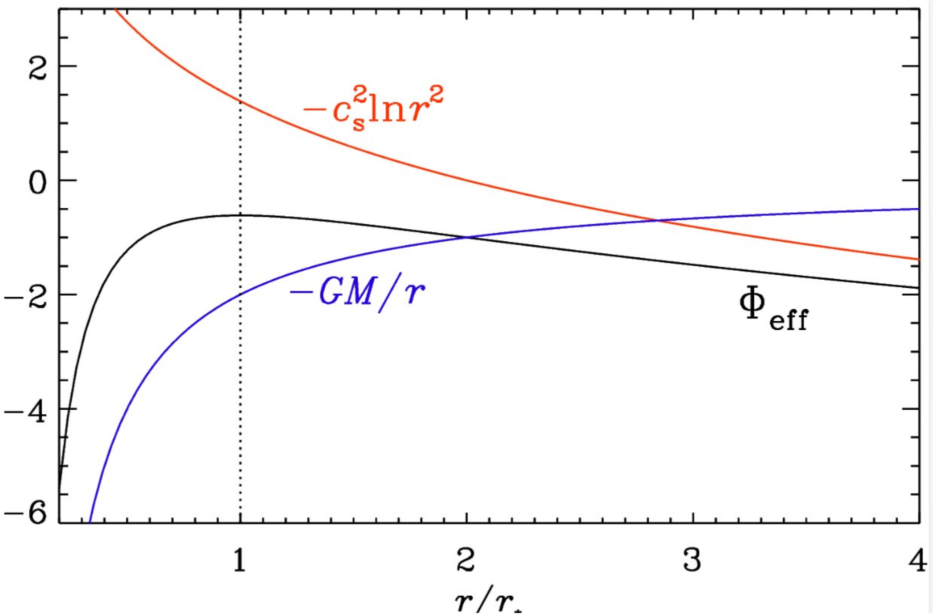

Fig. A.1. Effective potential $\Phi_{\text{eff}} = -c_s^2 \ln r^2 - GM/r$ (black), together with the Bernoulli term $-c_s^2 \ln r^2$ (red), and the gravitational potential $-GM/r$ (blue).

The model

Sun parameters:

$$c_s = 10^7\,\mathrm{cm\,s^{-1}} = 100\,\mathrm{km\,s^{-1}},$$

$$GM = GM_\odot \approx 1.3\times10^{26}\,\mathrm{cm^3\,s^{-2}},$$

$$r_* = GM_\odot/2c_s^2 \approx 7\times10^{11}\,\mathrm{cm} \approx 10R_\odot \approx 0.05\,\mathrm{AU}.$$

$$r_* = c_s = \dot{M}_0 = \mu_0 = 1$$

$$\Omega = 3\times10^{-6}\,\mathrm{s^{-1}}$$

$$\tilde{\Omega} = r_*\Omega/c_s = GM\Omega/2c_s^3 \approx 0.2,$$

$$\nu_T \approx u_{\mathrm{rms}}\ell/3 \approx 10^{13}\,\mathrm{cm^2\,s^{-1}}$$

$$\tilde{\nu}_T \equiv \frac{2\nu_T c_s}{GM_\odot} \approx 2\times10^{-6},$$

$$\dot{M}_0 \approx 6\times10^{12}\,\mathrm{g\,s^{-1}}$$

$$[\rho] = \dot{M}_0/c_s r_*^2 \approx 1.2\times10^{-18}\,\mathrm{g\,cm^{-3}}$$

$$[B] = (\mu_0[\rho])^{1/2}c_s \approx 0.04\,\mathrm{G}$$

Results

Model	$\tilde{\alpha}$	Q_α	$\tilde{\Omega}$	C_α	C_Ω	$\overline{B}_{\rm max}$	$P_{\rm cyc}$
A	0.05	10^{-2}	0.2	125	75	6–13	41.0
B	0.1	10^{-2}	1	250	375	16.0	—
C	0.1	10^{-1}	10	250	3750	8.8	—

Dynamo numbers:

$$C_\alpha = \alpha_0 R/\eta_{\rm T} \quad \text{and} \quad C_\Omega = \Delta\Omega R^2/\eta_{\rm T}. \qquad (20)$$

Results

- Mass loss

Local mass loss density:

$$\dot{M}(r,\theta,t) = 4\pi r^2 \overline{\rho}(r,\theta,t)\,\overline{U}_r(r,\theta,t),$$

Cumulative mass:

$$M_r(r,\theta,t) = \int_r^{\infty} 4\pi r'^2 \overline{\rho}(r',\theta,t)\,dr',$$

The mass above the surface is about 10, so 99.9% of the total mass in the computational domain is contained in the stellar envelope in $r_{in} \leq r \leq R$

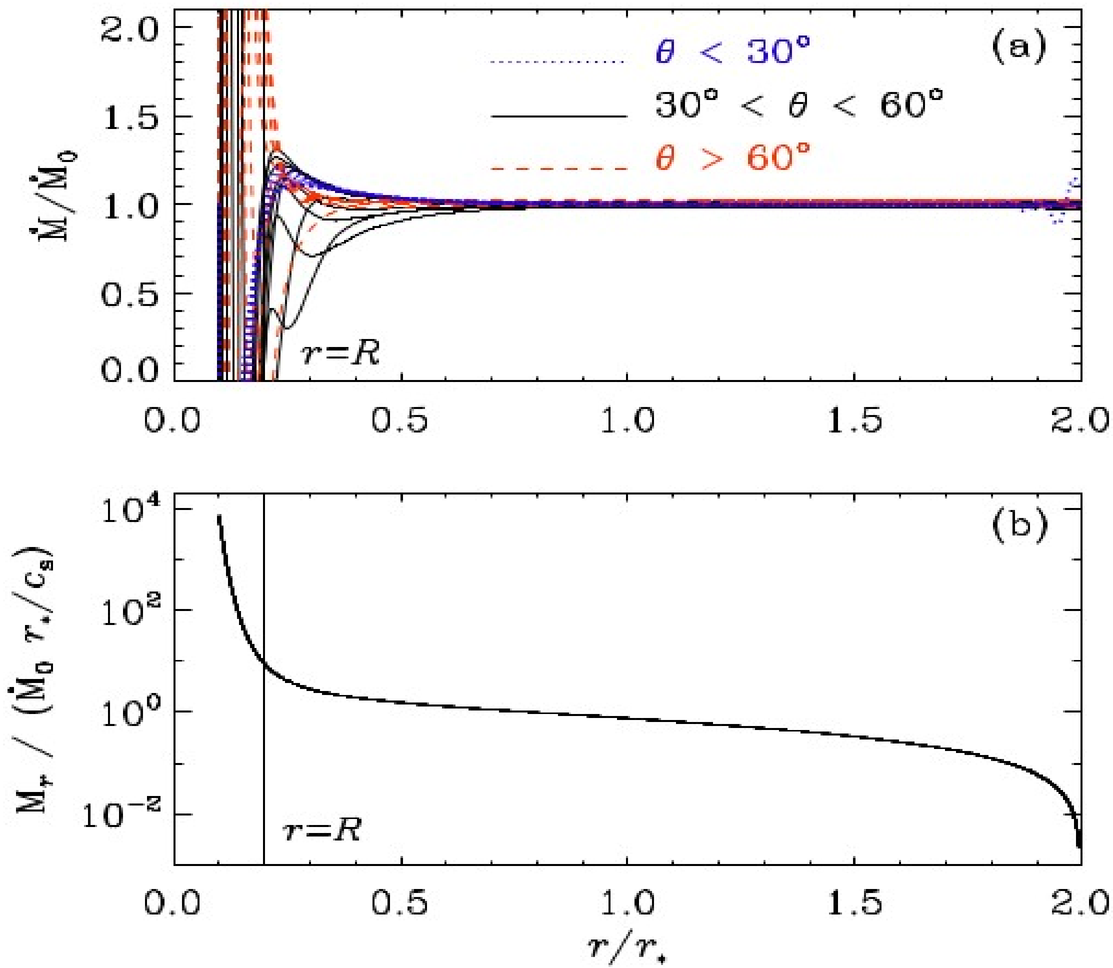

Fig. 1. Radial dependence of $\dot{M}$ (a) and M_r (b) for Model A.

Results

Oscillatory model at solar rotation rate

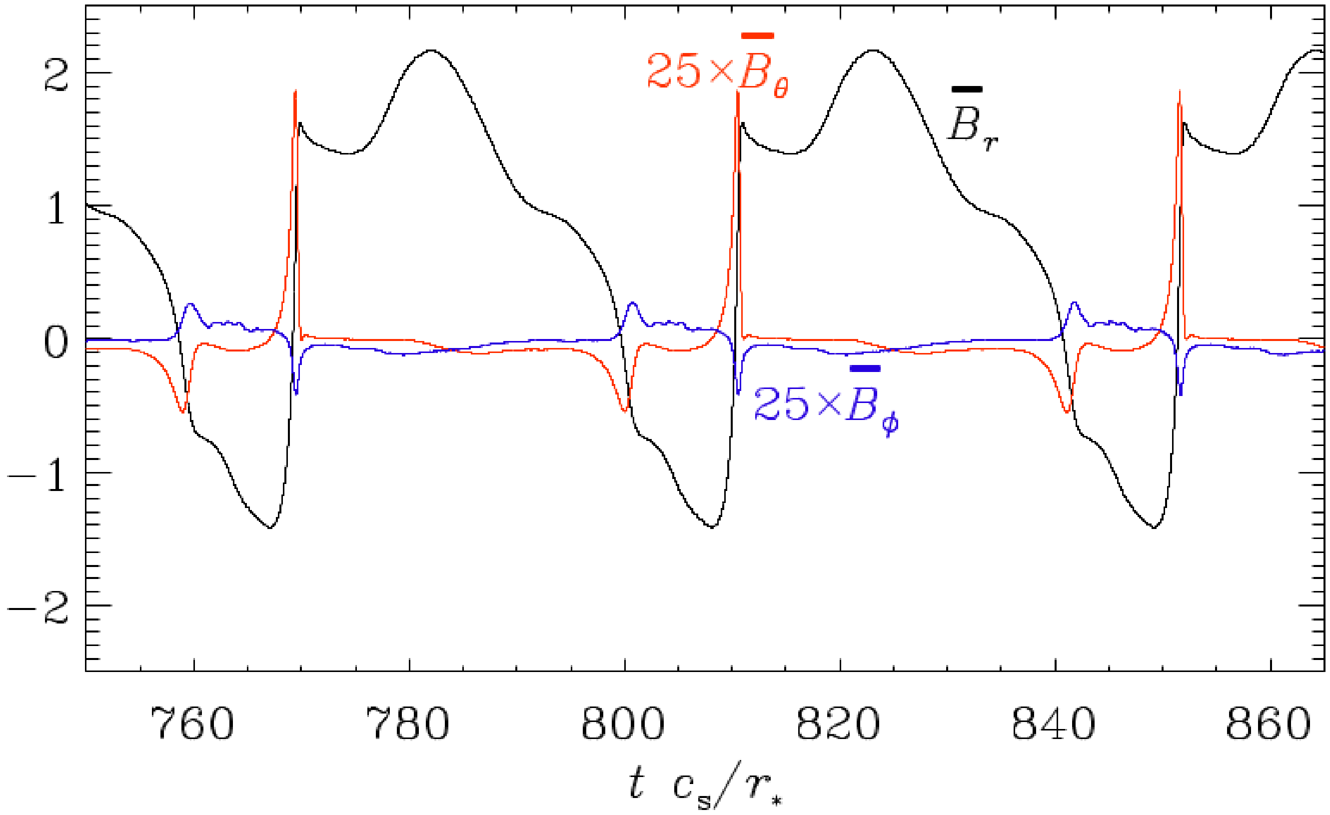

Fig. 2. Time series of the three magnetic field components at one point for Model A.

Results

Magnetic field geometry

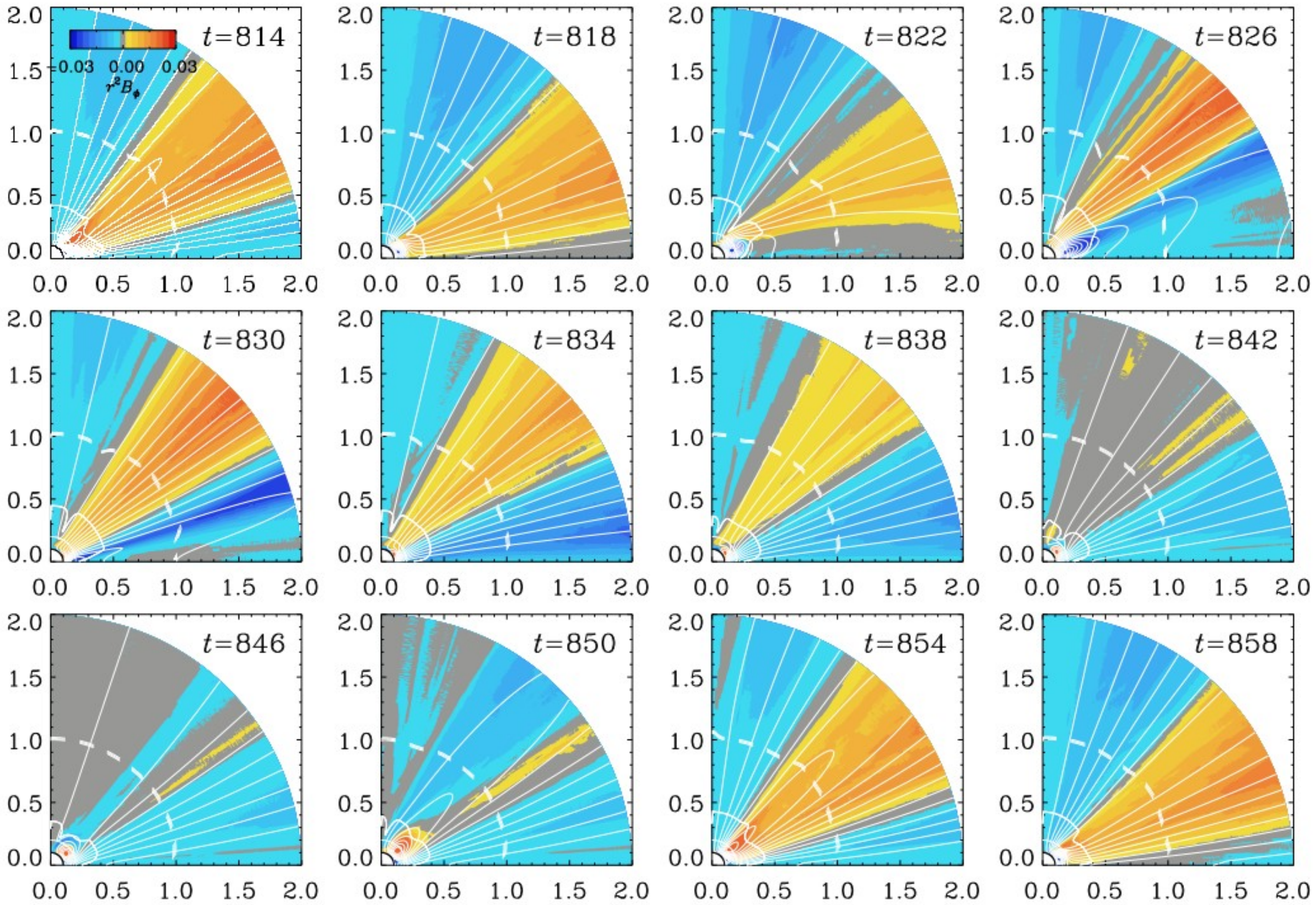

Fig. 3. Color representation of $r^2 B_\phi(r,\theta)$ for different times for Model A. The nearly concentric white solid lines show the surfaces where $\overline{U}_r$ is transonic and the dashed ones show the surfaces where it is transmagnetosonic.

We overplot the surfaces where $\overline{U}_r$ is transonic (solid white lines), i.e., where $\overline{U}_r$ exceeds the Alfvén speed $v_A = (\overline{\mathbf{B}}^2 / \mu_0 \overline{\rho})^{1/2}$. We also shows the surfaces where $\overline{U}_r$ is transmagnetosonic, i.e., where $\overline{U}_r$ exceeds the fast magnetosonic speed c_{ms} (dash white line), which obeys $c_{ms}^2 = c_s^2 + v_A^2$.

Results

Magnetic field geometry

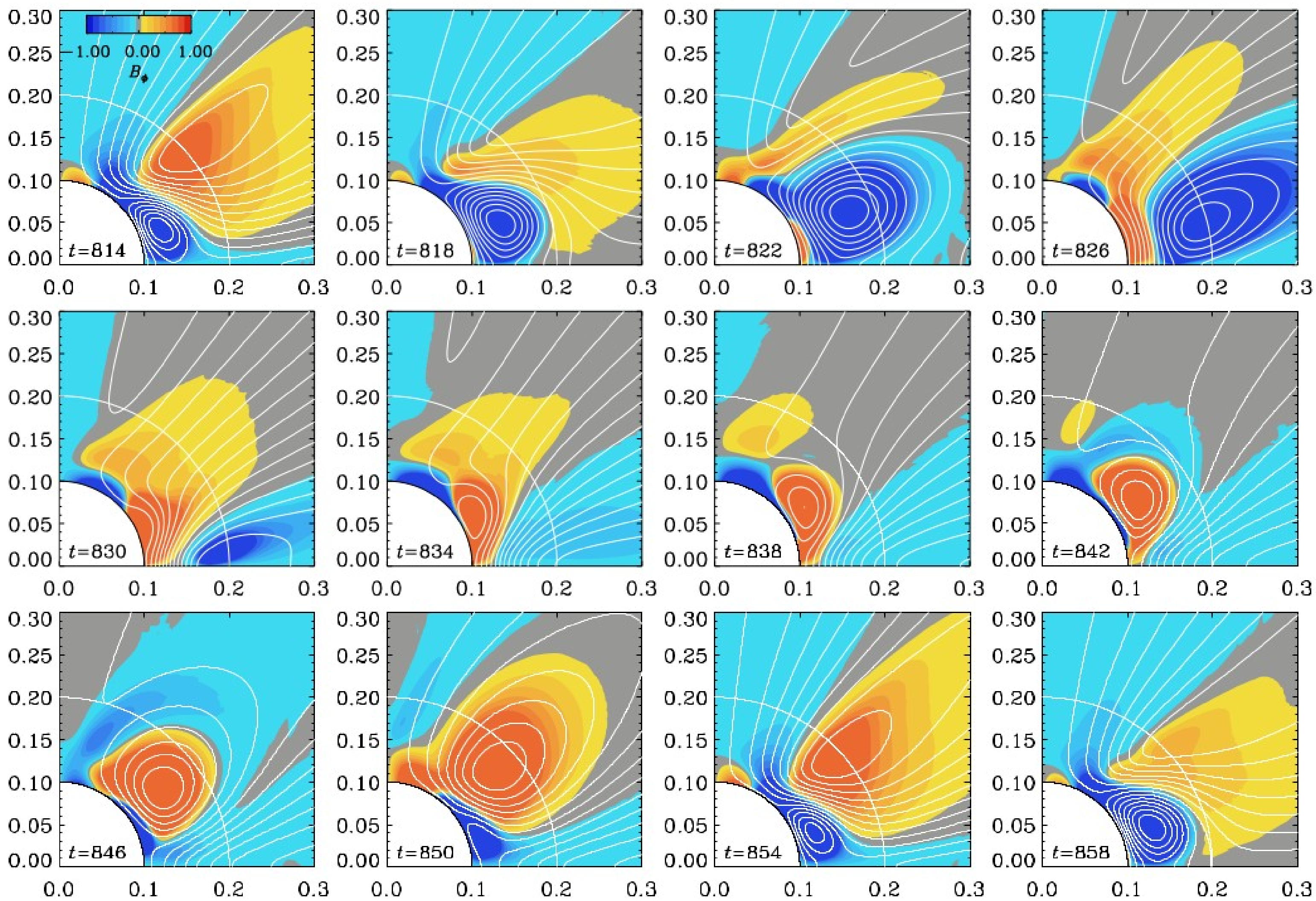

Fig. 5. Similar to Figure 3, but this time with a color representation of $B_\phi(r, \theta)$ showing only the region close to the center.

-periodicity with the period $P_{cyc} = 41$

Magnetic field geometry

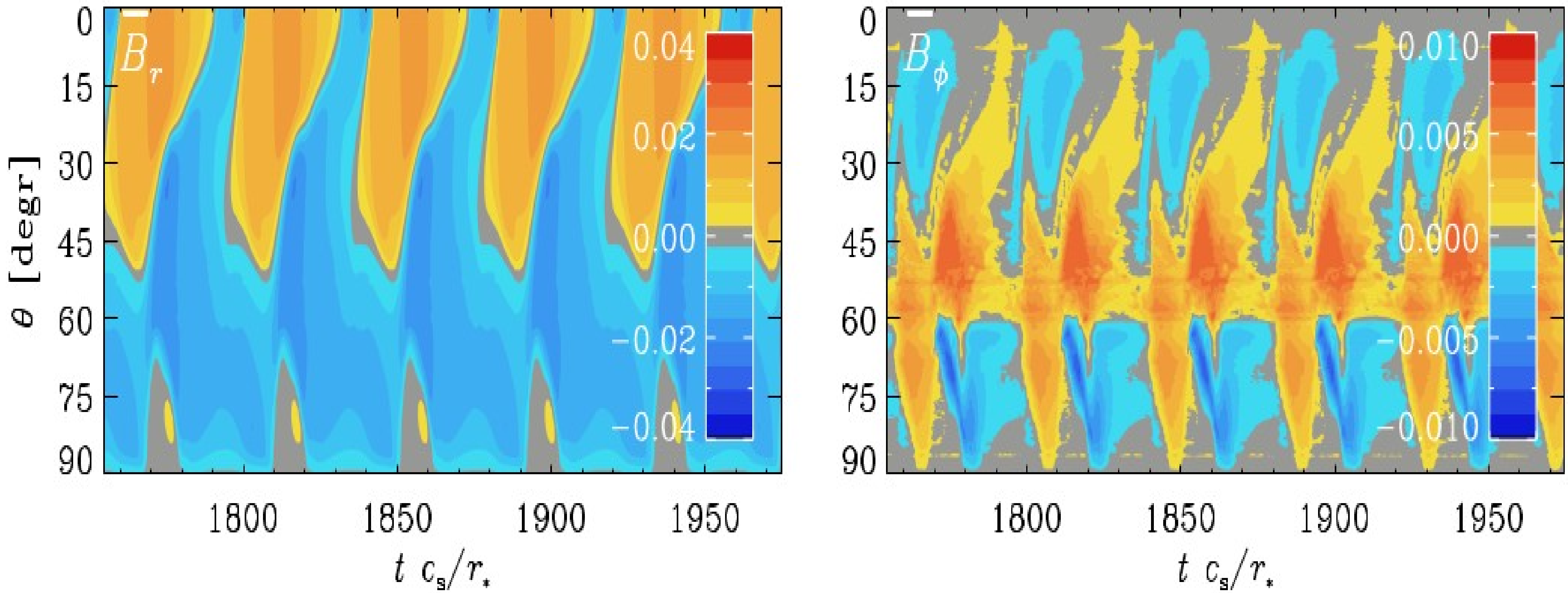

Fig. 4. Butterfly diagrams of $B_\phi(r,\theta)$ and $B_r(r,\theta)$ for Model A at $r/r_* = 1.9$.

Results

Poynting flux

$$F_{\rm Poy}(r,t) = \oint (\overline{\boldsymbol{E}} \times \overline{\boldsymbol{B}}/\mu_0) \cdot d\boldsymbol{S}, \qquad (29)$$

Mean electric field:

$$\overline{\boldsymbol{E}} = \mu_0 \eta_{\rm T} \overline{\boldsymbol{J}} - \alpha \overline{\boldsymbol{B}} - \overline{\boldsymbol{U}} \times \overline{\boldsymbol{B}}$$

Magnetic energy loss:

$$\dot{E}_{\rm M} = 4\pi r^2 F_{\rm Poy}.$$

-latitudinal dependence
energy loss

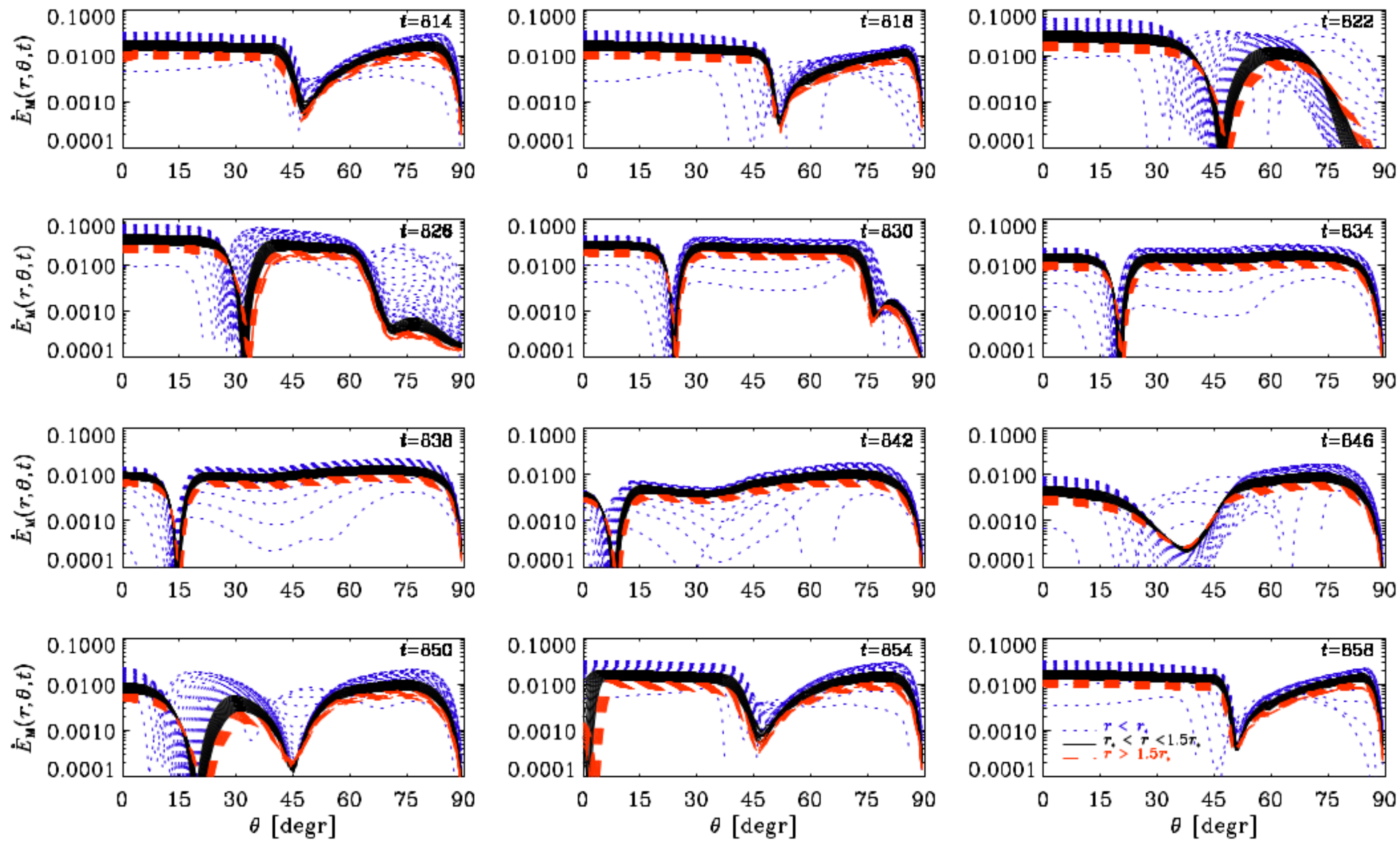

Fig. 6. Latitudinal dependence of the magnetic energy loss at different times for Model A.

Results

Poynting flux

Kinetic energy loss: $$\dot{E}_{\mathrm{K}} = 4\pi r^2 (\overline{\rho}\overline{U}^2/2)\, u_r, \tag{30}$$

Magnetic energy loss: $$\dot{E}_{\mathrm{M}} = 4\pi r^2 (\overline{B}^2/2\mu_0)\, u_r, \tag{31}$$

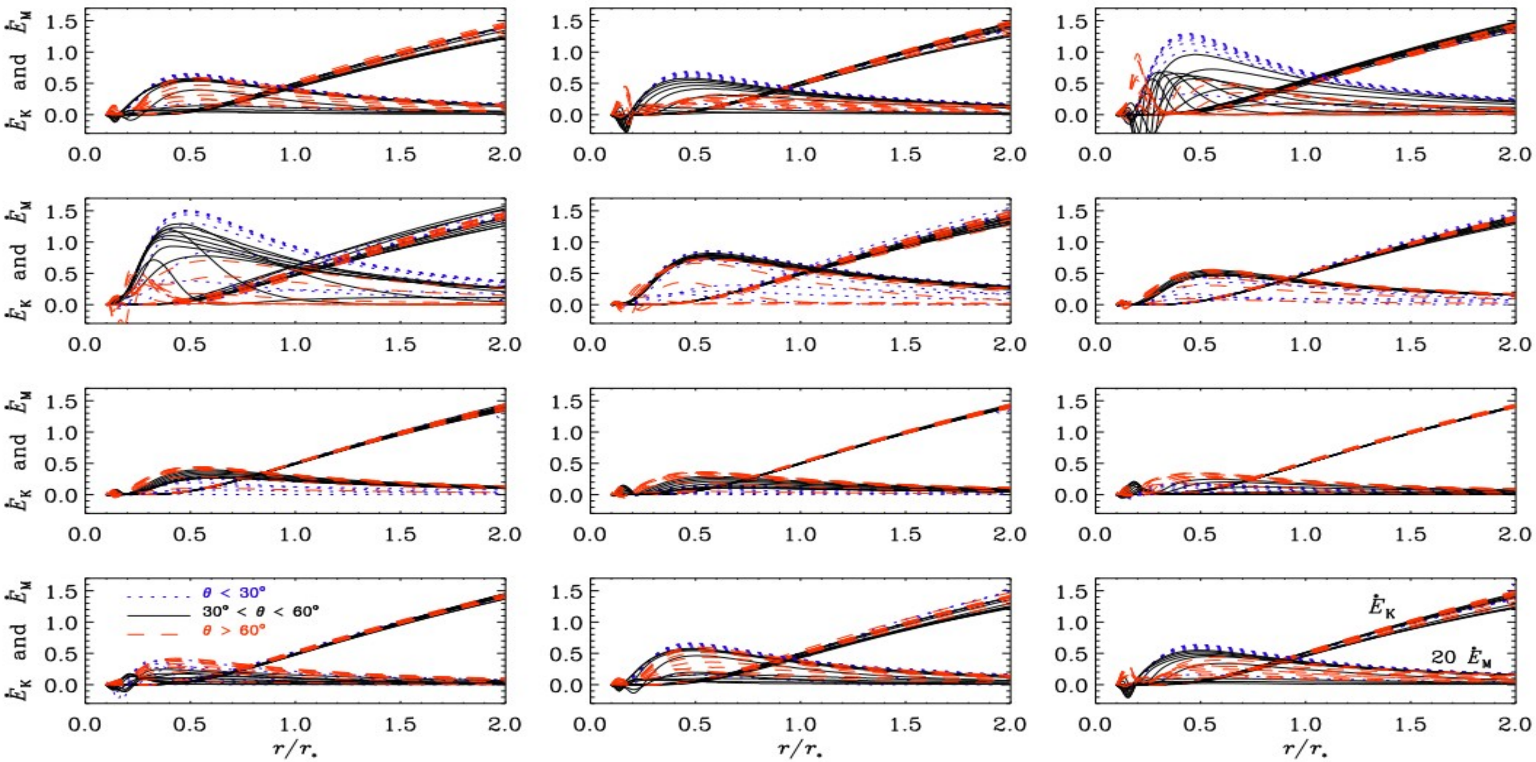

Fig. 7. Radial dependence of the magnetic and kinetic energy losses at different times for Model A. Note that $\dot{E}_{\mathrm{M}}$ has been multiplied by a factor of 20.

-kinetic energy loss is more dominant at the large radii

Results

Poynting flux

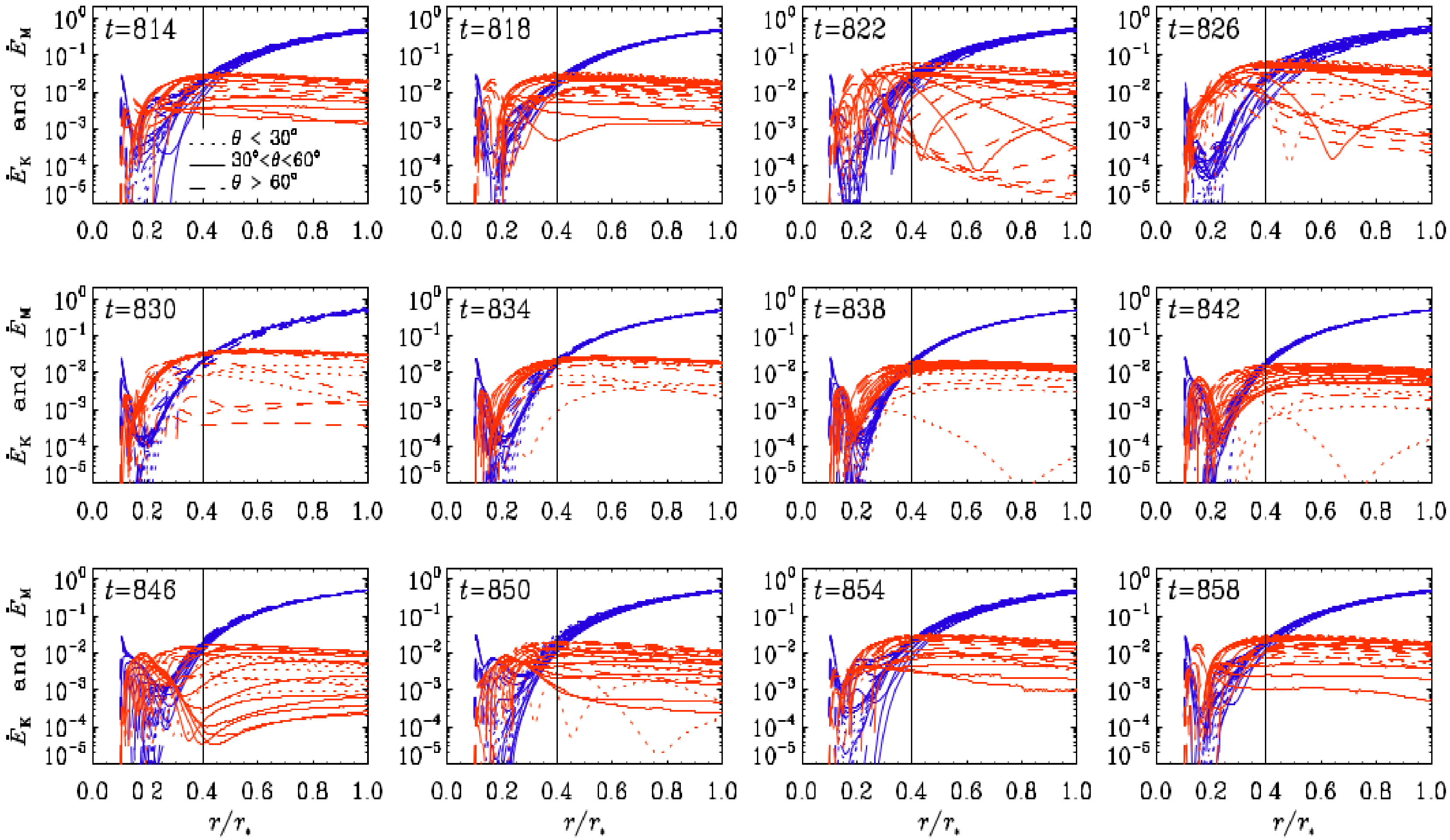

-kinetic and magnetic energy losses are equal at Alfvén point

Fig. 8. Similar to Figure 7, for a semilogarithmic representation, without having rescaled $\dot{E}_M$. Blue (red) lines indicate kinetic (magnetic) energy losses. Note that $\dot{E}_M \approx \dot{E}_K$ at $r/r_* \approx 0.4$.

Results

Angular momentum flux

$$\boldsymbol{F}^{\mathrm{AM}} = \overline{\rho}\varpi^2\Omega\overline{\boldsymbol{U}} - \varpi\overline{B}_\phi\overline{\boldsymbol{B}}/\mu_0 - \overline{\rho}\nu_\mathrm{T}\varpi^2\boldsymbol{\nabla}\Omega \qquad (33)$$

Angular momentum loss: $\dot{J} = 4\pi r^2 F_r^{\mathrm{AM}},$

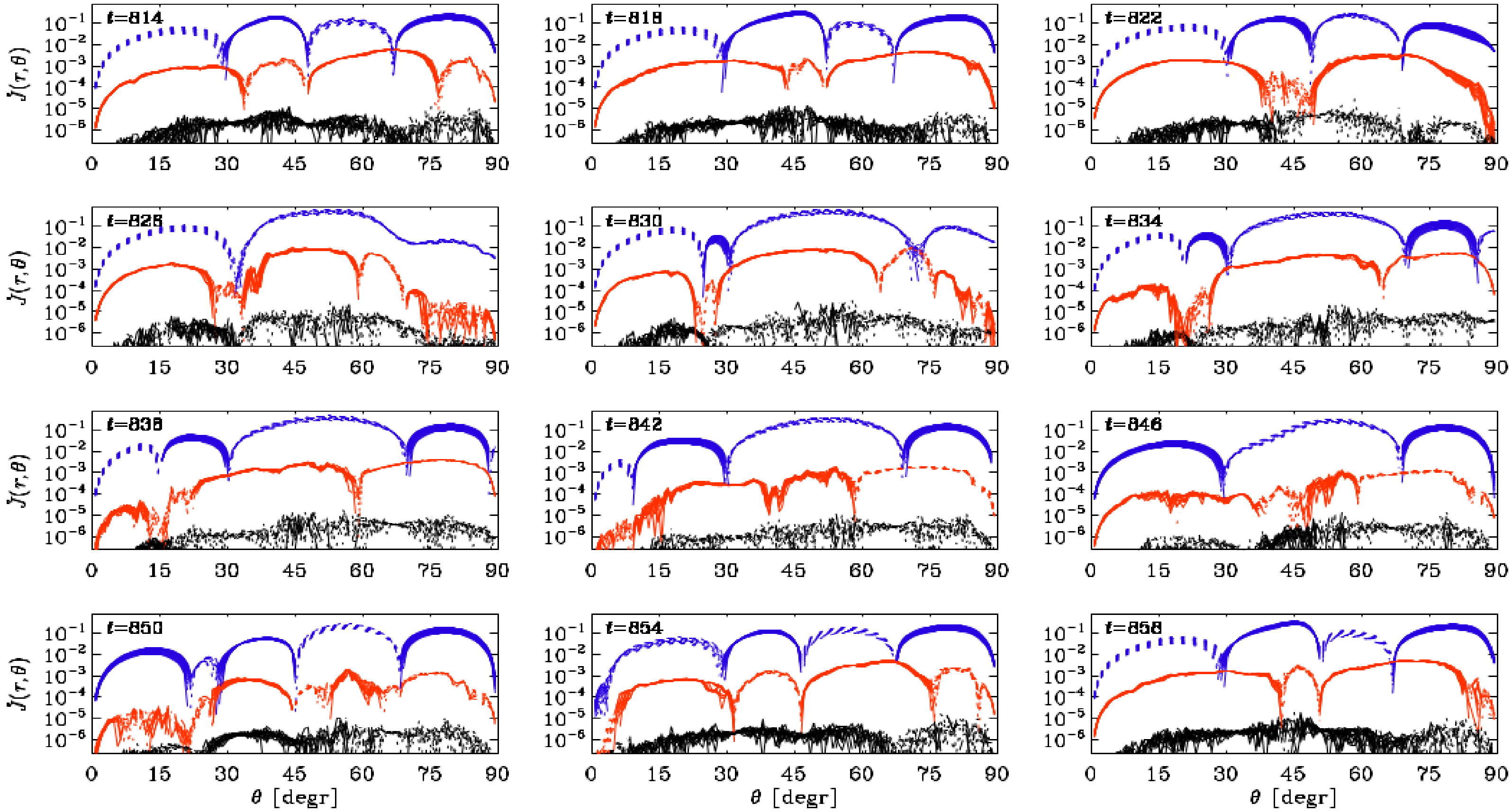

-sign changes in latitude and time

Fig. 9. Latitudinal dependence of the angular momentum loss $\dot{J}(r, \theta, t)$ at different times for Model A. The blue (red) lines refer to kinetic (magnetic) contributions, and the black lines denote the turbulent viscous contribution. Positive (negative) values are shown as solid (dotted) lines.

Results

Rapid rotation

For rapid rotation, the magnetic field lines and contours of the toroidal magnetic field are much more concentrated to the bottom of the dynamo region, $r \approx r_{in}$.

At faster rotation, the contours become more cylindrical. This is an effect of the Taylor–Proudman theorem and results generally in small variations along the rotation axis.

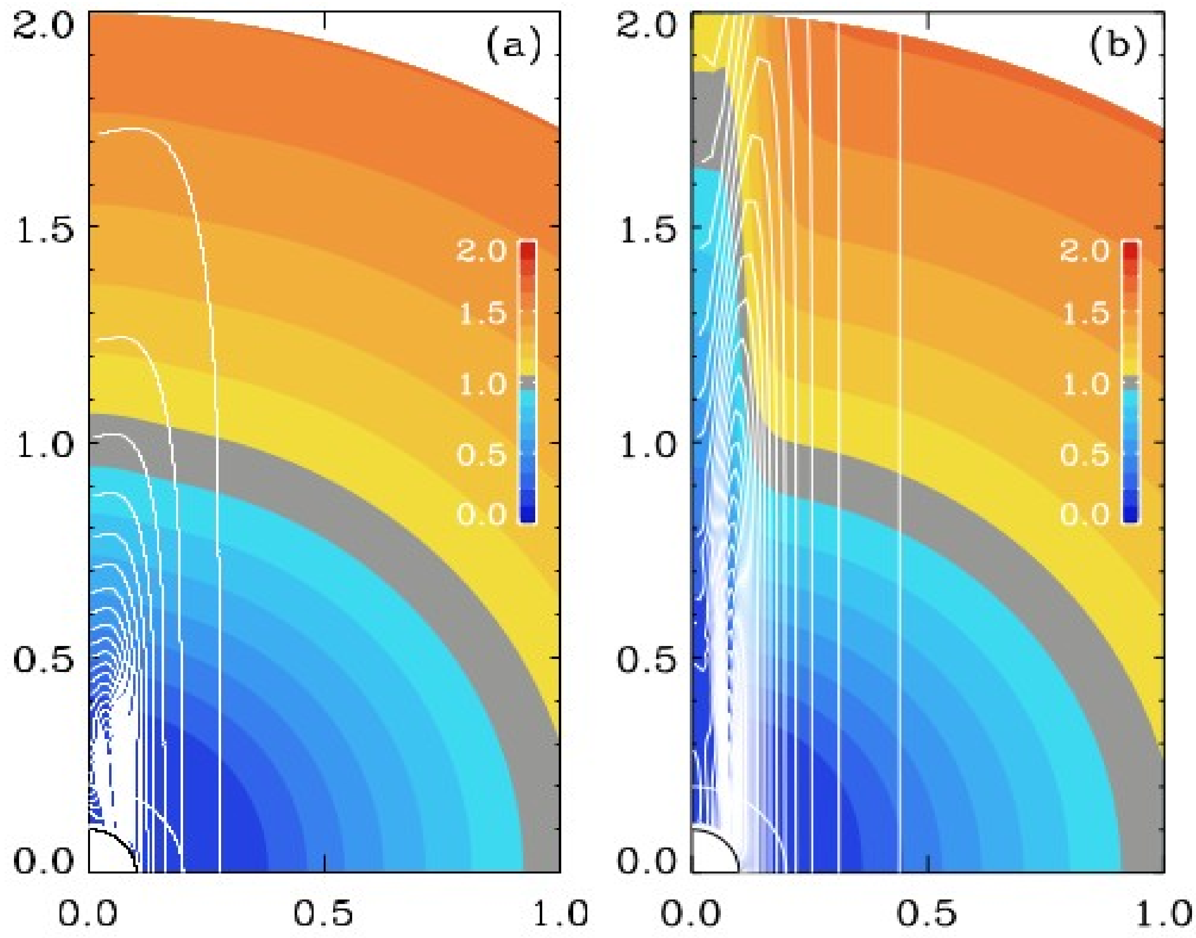

Fig. 10. Angular velocity contours superimposed on a color representation of $\overline{U}_r(r,\theta)$ for Model B (a) with $\tilde{\Omega} = 1$ and Model C (b) with $\tilde{\Omega} = 10$.

Results

Rapid rotation

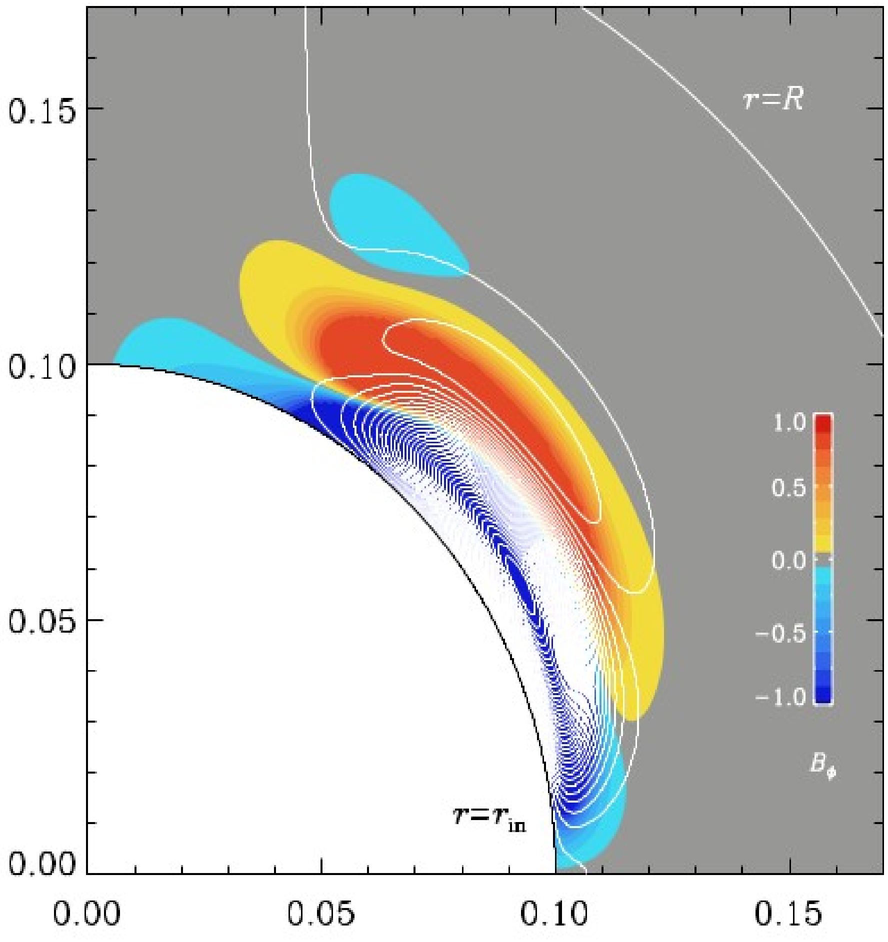

Fig. 11. Magnetic field lines superimposed on a color representation of $\overline{B}_\phi(r,\theta)$ for Model B with $\tilde{\Omega} = 1$.

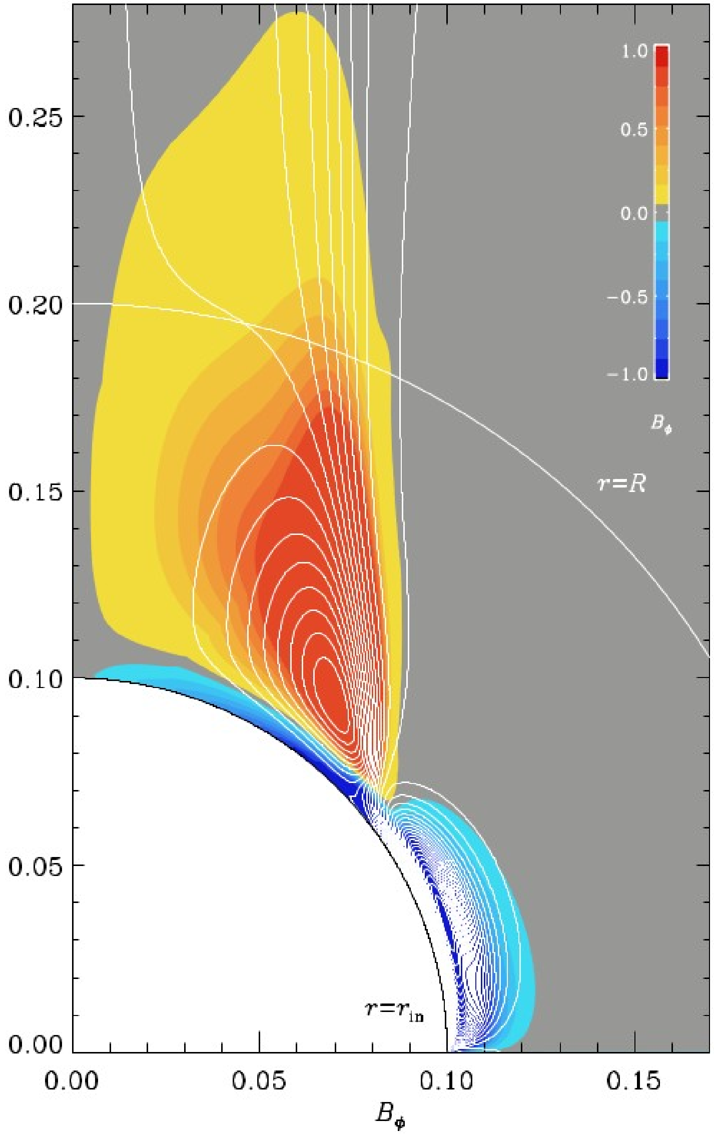

Fig. 12. Similar to Figure 11, but for Model C with $\tilde{\Omega} = 10$.

Results

Rapid rotation

The magnetic activity is confined to a narrow cone with an opening angle of about 15° . Noticeable magnetic energy losses are found only near the rotation axis.

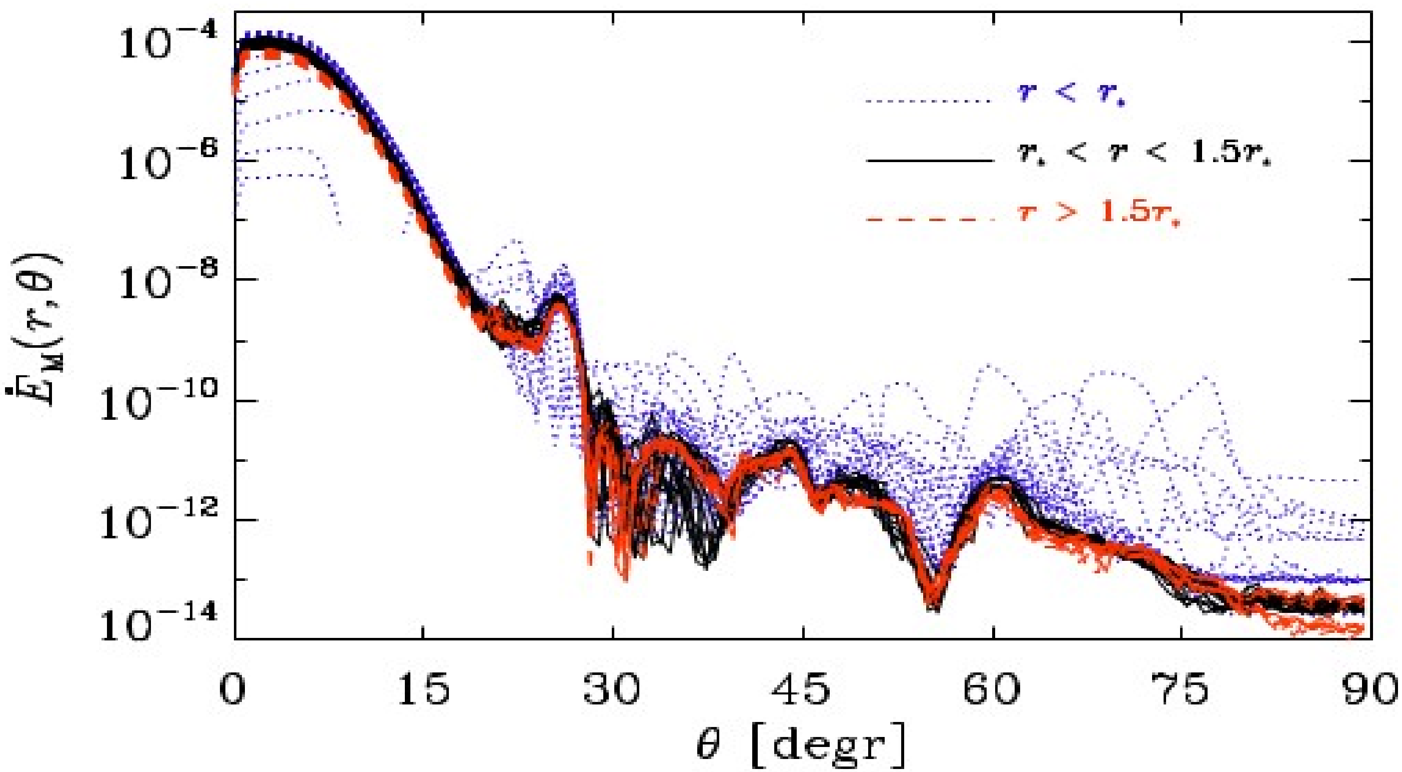

Fig. 13. Latitudinal dependence of the magnetic energy loss for Model B.

Results

Rapid rotation

$\dot{E}_M(r)$ has a maximum somewhere in $R < r < r_*$, which is where the Alfvén point lies. Model B has a much smaller magnetic energy loss at large radii than Model A

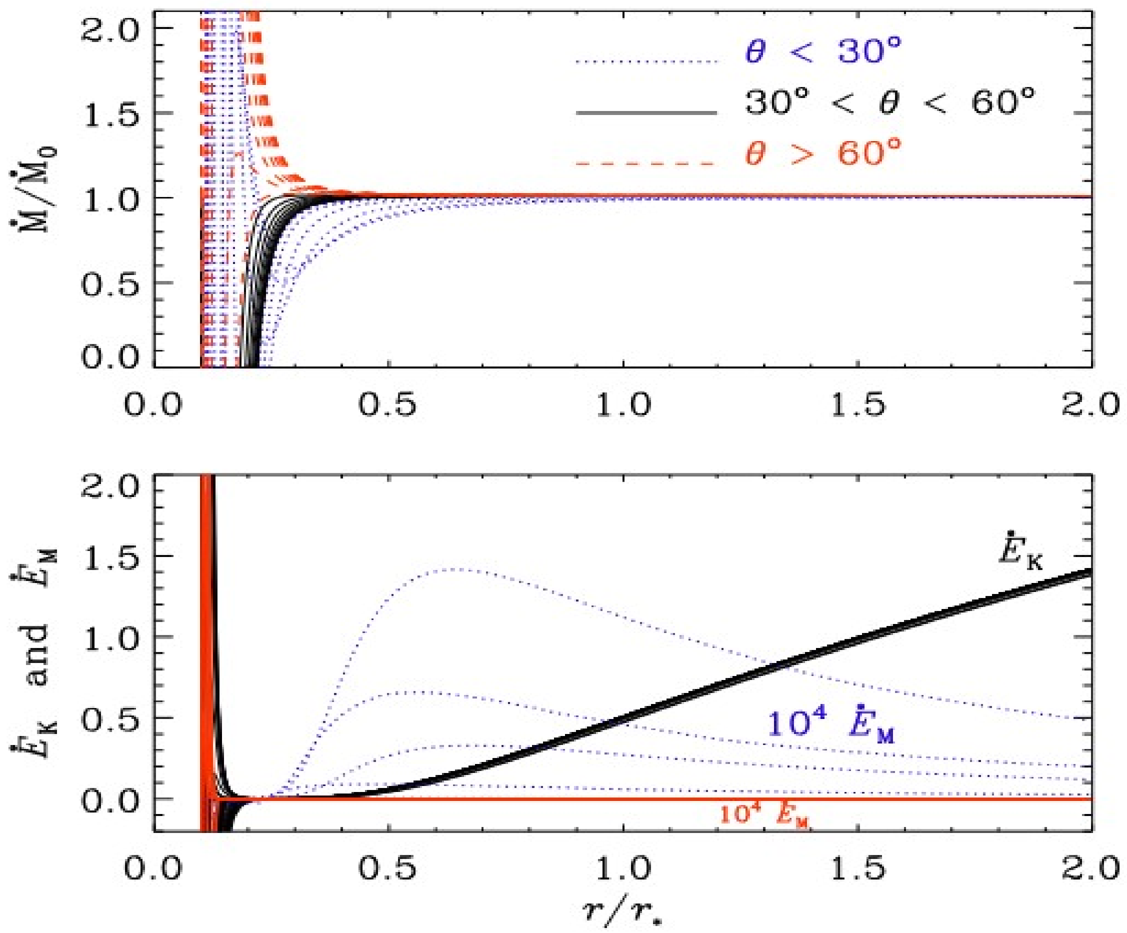

Fig. 14. Radial dependence of $\dot{M}$ (a) and $\dot{E}_M$ (b) for $0 \leq \theta \leq 30$ (close to the axis) as blue dotted lines, $30 \leq \theta \leq 60$, as black solid lines, and $60 \leq \theta \leq 90$ (close to the equator) as red dashed lines for Model B. The radial dependence of $\dot{E}_K$ is shown as green solid lines.

Conclusions

- simplified realization of a dynamo with a stellar wind
- the assumption of an isothermal equation of state has simplified matters conceptionally
- relatively large turbulent magnetic diffusivity and viscosity - mainly needed to resolve shocks that develop within the wind

Future work:

- inclusion of a Λ effect (Rüdiger,1980, 1989), which would allow for the development of differential rotation in the stellar envelope and might allow us to model the stellar dynamo more realistically, allow us to study dynamos in the $\alpha\Omega$ regime

References

Biermann, L. 1951, Z. f. Ap., 29, 274

Brandenburg, A., & Subramanian, K. 2005, Phys. Rep., 417, 1

Brandenburg, A., Moss, D., Rüdiger, G., & Tuominen, I. 1990, Solar Phys., 128, 243251

Brandenburg, A., Moss, D., Rüdiger, G., Tuominen, I. 1991, Geophys. Astrophys. Fluid Dyn., 61, 179

Brandenburg, A., Moss, D., & Tuominen, I. 1992, A&A, 265, 328

Brandenburg, A., Subramanian, K., Balogh, A., & Goldstein, M. L. 2011, ApJ, 734, 9

Chamberlain, J. W. 1960, ApJ, 131, 47

Cole, E., Brandenburg, A., Käpylä, P. J., & Käpylä, M. J. 2016, A&A, 593, A134

Del Sordo, F., Guerrero, G., & Brandenburg, A. 2013, MNRAS, 429, 1686

Frank, J., King, A. R., & Raine, D. J. 1992, Accretion power in astrophysics (Cambridge: Cambridge Univ. Press)

Gastine, T., Yadav, R. K., Morin, J., Reiners, A., & Wicht, J. 2014, MNRAS, 438, L76

Jabbari, S., Brandenburg, A., Kleeorin, N., Mitra, D., & Rogachevskii, I. 2015, ApJ, 805, 166

Käpylä, P. J., Käpylä, M. J., & Brandenburg, A. 2014, A&A, 570, A43

Krause, F., & Rädler, K.-H. 1980, Mean-field Magnetohydrodynamics and Dynamo Theory (Oxford: Pergamon Press)

Malkus, W. V. R., & Proctor, M. R. E. 1975, J. Fluid Mech., 67, 417

Mestel, L. 1968, MNRAS, 138, 359

Mestel, L. 1999, Stellar Magnetism (Clarendon Press, Oxford)

Metcalfe, T. S., & van Saders, J. 2017, Solar Phys., 292, 126

Mitra, D., Moss, D., Tavakol, R., & Brandenburg, A. 2011, A&A, 526, A138

Parker, E. N. 1958, ApJ, 128, 664

Perri, B., Brun, A. S., Réville, V., & Strugarek, A. 2018, J. Plasma Phys., 84, 765840501

Réville, V., Brun, A. S., Matt, S. P., Strugarek, A., & Pinto, R. F. 2015, ApJ, 798, 116

Roberts, P. H. 1972, Phil. Trans. R. Soc., A272, 663

Rüdiger, G. 1980, Geophys. Astrophys. Fluid Dyn., 16, 239

Rüdiger, G. 1989, Differential rotation and stellar convection: Sun and solar-type stars (Gordon & Breach, New York)

See, V., Matt, S. P., Finley, A. J., Folsom, C. P., Boro Saikia, S., Donati, J.-F., Fares, R., Hébrard, É. M., Jardine, M. M., Jeffers, S. V., Marsden, S. C., Mengel, M. W., Morin, J., Petit, P., Vidotto, A. A., Waite, I. A., the BCool Collaboration 2019, ApJ, 886, 120

Shakura, N. I., & Sunyaev, R. A. 1973, A&A, 24, 337

Shore, S. N. 1992, An introduction to astrophysical hydrodynamics (San Diego: Academic Press)

Stix, M. 1974, A&A, 37, 121

van Saders, J. L., Ceillier, T., Metcalfe, T. S., Silva Aguirre, V., Pinsonneault, M. H., García, R. A., Mathur, S., & Davies, G. R. 2016, Nature, 529, 181

von Rekowski, B., Brandenburg, A., Dobler, W., & Shukurov, A. 2003, A&A, 398, 825

von Rekowski, B., & Brandenburg, A. 2004, A&A, 420, 17

Warnecke, J., Käpylä, P. J., Mantere, M. J., & Brandenburg, A. 2013, ApJ, 778, 141

Weber, E. J., & Davis, L., Jr. 1967, ApJ, 148, 217

Thank you for your attention.